Unravelling the synthesis of a rare-earth cluster-based metal–organic framework with spn topology

Hudson A. Bicalho,[†ab] Felix Saraci,[†ab] Jose de J. Velazquez-Garcia,[c] Hatem M. Titi,[d] Ashlee J. Howarth[ab]

Y-CU-45, an analogue of Zr-MOF-808, is synthesized for the first time. Several reaction conditions are tested demonstrating that two fluorinated modulators are required for a reproducible synthesis yielding high quality material. Y-CU-45 shows high crystallinity and surface area, shining light on the potential for rare-earth cluster-based MOFs with open metal sites.

Metal–organic frameworks (MOFs) are a class of multifunctional, porous materials[1, 2] with diverse structural tunability that can be used for various potential applications.[3-6] In addition to the many important potential applications of these materials, their beautiful network structures also allow for the study of various fundamental phenomena in inorganic and materials chemistry. MOFs are constructed from inorganic metal nodes and organic linkers (di-, tri-, tetratopic etc.) that assemble into 2D or 3D framework materials.[7] In that way, materials with targeted structures and properties can be synthesized due to the seemingly endless combinations of metal nodes and organic linkers that can be used as building blocks. Over the years, MOFs comprised of *s*-,[8] *p*-,[9] *d*,[10] and *f*-block[11] metals have been reported. Owing to their high and variable coordination numbers and geometries, the incorporation of rare-earth (RE) ions in MOFs has attracted significant interest, as unique structures can be realized. Among the materials that have been reported, MOFs comprised of RE ions have been shown to have diverse structures, with secondary buildings units (SBUs) that include metal ions, chains, or multinuclear clusters.[12]

The high coordination number of RE ions, particularly when coupled with the ability to form multinuclear cluster nodes, allows for the synthesis of intricate structures with complex topologies.[4] These unique structures arise, in part, from the ability to form highly connected (12-, 18-) metal nodes.[11] On the other hand, the design and synthesis of RE-cluster MOFs with lower node connectivity (8-, 6-) is less commonly observed due to difficulties associated with stabilizing under-connected multinuclear RE-clusters.[13] This is in contrast to the well-known Zr-based MOFs where frameworks with 4-, 6-, and 8-connected nodes have been studied for various applications where metal accessibility is an asset.[14]

First reported in 2014, MOF-808 is a MOF made of hexanuclear Zr-clusters connected by 1,3,5-benzenetricarboxylate (BTC) linkers, giving rise to a material with **spn** topology.[15] Due to the overall structure of the material, MOF-808 features six open metal sites per node that are capped by formate or terminal –OH and $–OH_2$ ligands,[15, 16] which makes this MOF appealing for many applications including catalysis and adsorption.[17, 18] However, up to this day,

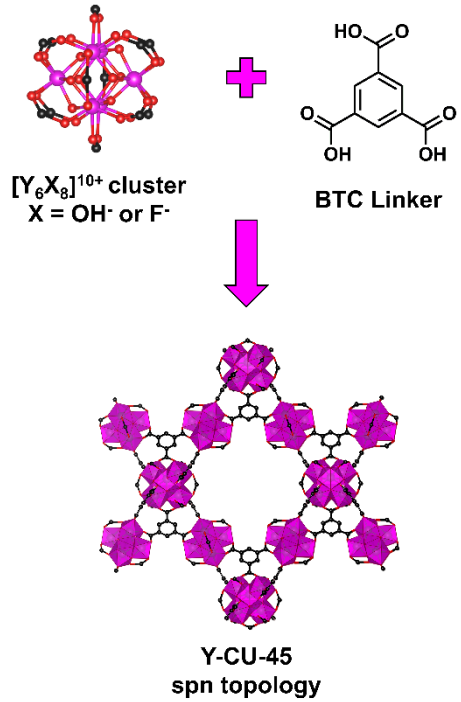

Figure 1. Structure of Y-CU-45 displaying the overall **spn** topology assembled by hexanuclear Y(III)-clusters and BTC linkers.

[a.] *Department of Chemistry and Biochemistry, Concordia University, 7141 Sherbrooke Street W., Montreal, QC, H4B 1R6*
[b.] *Centre for NanoScience Research, Concordia University, 7141 Sherbrooke Street W., Montreal, QC, H4B 1R6*
[c.] *Photo Science - Structural Dynamics in Chemical Systems, Deutsches Elektronen-Synchrotron DESY, Notkestraße 85, Hamburg, 22607, Germany*
[d.] *Department of Chemistry, McGill University, 801 Sherbrooke Street W., Montreal, QC, H3A 0B8*
† H.A.B. and F.S. contributed equally to this work
Email: ashlee.howarth@concordia.ca

there are no reports in the literature regarding the synthesis and isolation of RE analogues of MOF-808. This is most likely due to the difficulty in translating synthetic procedures from Zr-MOFs to RE-MOFs, which often requires changing several reaction parameters, including the type of modulator, reactant ratios, temperature, and time.[19, 20] Another possible reason for the shortage of under-connected RE-cluster nodes in the literature is the reported lack of thermodynamic stability of the hexanuclear RE-cluster with open metal sites, which has been suggested to undergo a rearrangement to yield RE-*oxo* chains.[13]

In our pursuit to obtain a RE analogue of MOF-808, henceforth denominated as Y-CU-45 (Fig. 1, CU = Concordia University), an exhaustive synthetic study was undertaken to determine the best parameters for a reproducible synthesis yielding high quality material. We started by using 2-fluorobenzoic acid (2-FBA), and 2,6-difluorobenzoic acid (2,6-dFBA) as modulators for the synthesis of Y-CU-45. According to previous findings in the literature,[12, 21] 2-FBA and 2,6-dFBA can act as structure directing agents for the formation of hexanuclear and nonanuclear clusters, in part due to hydrophobicity granted by the fluorine group(s), which help to avoid the formation of infinite RE-*oxo* chains. In addition to that, recent work by Vizuet *et al.*[22] suggests that fluorinated modulators are needed for the synthesis of cluster-based MOFs because these clusters are, in fact, connected by μ_3-F groups, instead of the originally thought μ_3-OH groups. Nevertheless, when 2-FBA and 2,6-dFBA were used as modulators in reactions with Y(III) salts and BTC, the final products were either amorphous or chain-based MOFs like Y-MOF-76[23] when only 2-FBA was used (Fig. S1), or a mixture of Y-MOF-76 and $Y_2(BTC)_2DMF(H_2O)$[24] when only 2,6-dFBA was used (Fig. S2).

Taking inspiration from standard synthetic procedures for Zr-MOF-808, where formic acid and acetic acid are often used as modulators,[25, 26] we hypothesized that trifluoroacetic acid (TFA) could be a potential modulator for the synthesis of Y-CU-45. After several synthetic attempts, it became clear that Y-CU-45 could indeed be obtained through this method but with poor reproducibility and often containing Y-MOF-76 as a mixed-phase product (Fig. S3). Seeking to circumvent this issue, 2-FBA and 2,6-dFBA were added as co-modulators, along with TFA, for the synthesis of Y-CU-45. While the combination of 2-FBA/TFA leads to products with higher crystallinity than those obtained using TFA alone, reproducibility was still a recurring problem due to the formation of mixed-phase materials (Fig. S4). On the other hand, when 2,6-dFBA and TFA were used as co-modulators, pure-phase Y-CU-45 crystals are the only product of the reaction (Fig. 2a). As shown in the powder X-ray diffraction patterns in Fig. 2a, all observed reflections match those expected for a MOF-808 analogue with the **spn** topology.[15] Crystallographic data obtained by synchrotron single crystal X-ray diffraction (SCXRD) demonstrates that Y-CU-45 crystallizes in the cubic space group, *Fd*$\bar{3}$*m*, with lattice parameter *a* = 36.079 Å (Table S1, S2 and Fig. S5). Furthermore, the crystal structure solution of Y-CU-45 confirms its overall **spn** topology assembled from 6-connected $[Y_6(\mu_3\text{-}X)_8(COO^-)_6]^{4+}$ (X = F^- or OH^-) SBUs. In a similar fashion to MOF-808, Y-CU-45 features tetrahedral cages of *ca.* 8 Å and large adamantane cages of *ca*. 18 Å. Variable temperature powder X-ray diffraction (VT-PXRD) measurements collected from 25 to 300 °C (Fig. S6 and S7) demonstrate that no other crystalline phase is generated in this temperature range. However, a substantial loss in crystallinity is observed at temperatures higher than 180 °C. This is in contrast to what is observed in RE-UiO-66, which contains a 12-connected hexanuclear cluster node, and the material remains stable to 200 °C.[20] This suggests that the 6-connected hexanuclear RE(III)-cluster node may be less stable at high temperatures than the 12-connected hexanuclear RE(III)-cluster node, somewhat consistent with previous reports on the lack of stability of under-connected RE-clusters.[13] In addition, corroborating the results obtained by PXRD and SCXRD, scanning electron microscopy (SEM) images (Fig. 2b and 2c) display the expected octahedral crystallites with average size of 25 µm.

To gain a better understanding of the coordination environment of the SBUs, a sample of Y-CU-45 was digested and ^1H and ^{19}F nuclear magnetic resonance (NMR) spectroscopy measurements were obtained (Fig. S8 and S9). After solvent exchange with DMF and acetone, NMR spectroscopy of the digested MOF shows peaks characteristic of 2,6-dFBA, TFA, and formate. Specifically, ratios of 2:3:1.5:1 are observed for BTC:2,6-dFBA:TFA:formate. Interestingly, the number of capping ligands aligns with the number of open metal sites dictated by the coordination number of Y(III) ions in the Y-CU-45 SBU, suggesting that 2,6-dFBA, TFA, and formate are coordinated to the Y_6-cluster node, rather than being present in excess in the pores. In this topology, each hexanuclear cluster is connected by six $-COO^-$ moieties from two BTC linkers, leaving

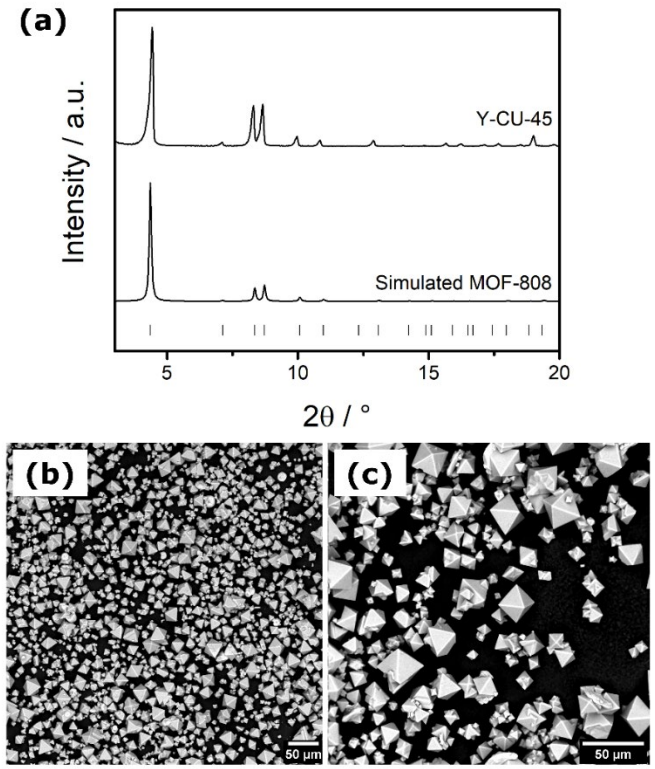

Figure 2. (a) PXRD patterns of Y-CU-45 and the calculated for Zr-MOF-808 and (b) and (c) SEM images of Y-CU-45.

four to six open metal sites based on charge or coordination number. According to the NMR spectroscopy data obtained, three open metal sites are coordinated to 2,6-dFBA, approximately two are coordinated to TFA, and one is coordinated to a formate ligand (Fig. S10). The resulting –2 charge of the framework may be balanced by dimethylammonium cations, dangling linkers, or missing linkers. In addition to that, an extra peak around 1.9 ppm in the ^{1}H NMR spectrum can be attributed to the presence of acetone, even after the activation of the MOF (*vide infra*). An additional singlet around -169 ppm is also observed in the ^{19}F NMR spectrum. This peak is not related to any of the modulators nor their degradation products. A similar singlet is also found in the ^{19}F NMR spectrum of digested Y-UiO-66 samples (Fig. S11), which seems to be additional evidence for the existence of μ_3-F groups in these hexanuclear RE-clusters.[22]

To further confirm the presence of the capping ligands in the MOF and the thermal stability of Y-CU-45, thermogravimetric analysis coupled to mass spectrometry and infrared spectroscopy (TGA-MS-IR) measurements were performed. As can be seen in the TGA curve (Fig. S12) five weight loss events can be observed from 30 to 800 °C. The first weight loss event starts at room temperature and finishes around 100 °C and can be attributed to the desorption of gases (*e.g.* O_2, CO_2, etc.) and water. The next weight loss event starts around 160 °C and finishes at 220 °C. According to the obtained IR spectroscopy and MS data (Fig. S13), this event is related to the release of trapped acetone from the pores of the MOF. Interestingly, according to the VT-PXRD results (Fig. S6 and S7), around the same temperature Y-CU-45 starts losing crystallinity. As such, it is possible that the removal of acetone from the pores of the MOF at these temperatures may be too harsh for the framework, leading to its partial collapse.[27] The third weight loss event starts at 300 °C and finishes at 420 °C. At this temperature, the species that is released from the MOF starts to partially carbonize, resulting in an intense band related to CO_2 in the IR spectrum (Fig. S14a). However, a pronounced band around 1150 cm^{-1} can be attributed to the C–F stretching vibration of TFA. The fourth weight loss event starts at 450 °C and finishes at 500 °C. Again, an intense band related to CO_2 can be observed in the IR spectrum (Fig. S15a) but other bands are also present. Specifically, a band at *ca.* 1600 cm^{-1} can be attributed to C=O stretching vibration. Associated to that, a fragment of *m/z* equal to 114 in the MS spectrogram (Fig. S15b) can be attributed to the fragmented $(C_6H_4F_2)^+$ group resulting from the loss of COO^- from 2,6-dFBA. Finally, the last mass loss event starts at 630 °C and is attributed to the decomposition of the remaining 2,6-dFBA molecules and BTC linker. Due to the high temperature, only CO_2 can be observed in the IR spectrum and MS spectrogram (Fig. S16).

In order to obtain the BET surface area of Y-CU-45, N_2 sorption measurements were carried out at 77 K. Different activation temperatures were tested (Fig. S17), seeking conditions that would give the highest BET surface area. In these experiments, samples of Y-CU-45 were heated under vacuum for 24 h at 50, 60, 80, 100, 110, and 130 °C, giving BET surface areas of 590, 1280, 880, 300, 40, and 20 m^2 g^{-1}, respectively. As previously observed from the VT-PXRD and TGA-MS-IR data, the removal of acetone from inside the pores of Y-CU-45 at *ca* 160-180 °C leads to a decrease in crystallinity of the material. Since the surface area decreases when the sample is heated under vacuum at temperatures higher than 60 °C, it can be assumed that acetone is being removed from the pores of Y-CU-45, leading to the partial collapse of the framework. Comparably, heating the sample at temperatures lower than 60 °C under vacuum may lead to incomplete removal of the superficially adsorbed acetone and other molecules, resulting in low apparent surface areas.

Given that Zr-MOF-808 displays surface areas in the range of 1600–2100 m^2 g^{-1},[26] the maximum obtainable surface area for Y-CU-45 is expected to be higher than 1280 m^2 g^{-1}. We hypothesized that the capping ligands 2,6-dFBA, TFA, and formate partially block the pores of Y-CU-45, resulting in less accessible pores (particularly the 8 Å pore) and lower surface areas. Indeed, the simulated pore size distribution demonstrates that the large adamantane cages (*ca.* 18 Å) are partially blocked, giving rise to pores of 15.5 Å in size (Fig. S18). The same phenomenon is observed for other MOFs such as NU-1000 and PCN-222.[28, 29] In these cases, the MOF is washed with an acidic solution to displace the capping ligands and render the open metal sites accessible. As such, different acid washing conditions were tested for Y-CU-45 (Fig. S19) and it was found that acid washing of the as-synthesized MOF can promote a considerable increase in BET surface area. Specifically, after the acid washing, the material still shows the characteristic type Ib isotherm, but with BET surface area of 1570 m^2 g^{-1} (Fig. 3). The pore size distribution analysis also demonstrates that the larger pores are no longer partially blocked, as only the expected pore of 18.4 Å is observed. In addition, after acid washing the material still shows high crystallinity, with a diffraction pattern similar to the non-acid washed Y-CU-45 MOF (Fig. S20).

^{1}H and ^{19}F NMR spectroscopy measurements of the acid washed samples (Fig. S21-S26) demonstrate that washing the

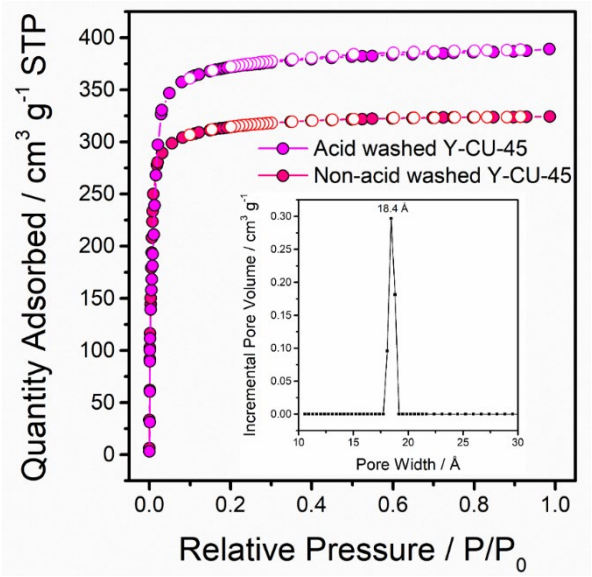

Figure 3. N_2 sorption isotherms of the acid washed and non-acid washed Y-CU-45 samples with inset of pore size distribution for the acid washed Y-CU-45.

samples with 0.1 M HCl for 1, 2, and 3 days leads to an increasing removal of the capping ligands. While the as-synthesized Y-CU-45 displays ratios of 2:3:1.5:1 for BTC:2,6-dFBA:TFA:formate, respectively, the samples washed for 1, 2, and 3 days with 0.1 M HCl show ratios of 2:1.7:1:0.5, 2:0.8:0.6:0.5, and 2:0.4:0.3:0.5, respectively, for BTC:2,6-dFBA:TFA:formate. This suggests that each acid wash removes approximately half of the capping ligands (especially 2,6-dFBA and TFA), in comparison to the previous wash. However, after the second acid wash, the surface area decreases from 1570 m^2 g^{-1} to 870 m^2 g^{-1} and 580 m^2 g^{-1} (for 2 and 3 days, respectively), indicating a partial collapse of the framework after removal of more than 50% of the capping ligands. Moreover, TGA of the as-synthesized and acid washed sample shows that the organic component of Y-CU-45 decomposes at approximately 500 °C, while also confirming the partial removal of capping ligands in the acid washed sample (Fig. S27). Consistent with NMR spectroscopy data, TGA of the acid washed sample (0.1 M, 1 day) shows approximately half the weight loss during the mass loss events previously ascribed to TFA and 2,6-dFBA.

In conclusion, we report here a novel RE-MOF composed of hexanuclear Y_6-clusters and tritopic BTC linkers to give Y-CU-45, a MOF analogous to Zr-MOF-808. A mixture of two fluorinated modulators, 2,6-dFBA and TFA, is used for the first time for the synthesis of a RE-MOF. Characterization data demonstrate that octahedral crystallites with the expected **spn** topology were successfully obtained, displaying surface areas as high as 1570 m^2 g^{-1}. NMR spectroscopy and TGA-MS-IR measurements show the presence of capping ligands (2,6-dFBA, TFA, and formate) in the material, which are coordinated to the open metal sites of the MOF node. An acid washing procedure can be carried out to partially remove these capping ligands without compromising the framework, making Y-CU-45 the first example of a RE-MOF with 6-connected hexanuclear cluster nodes, and the potential for a high density of open metal sites.

HAB thanks Concordia University and the Fonds de Recherche du Québec – Nature et technologies for providing doctoral scholarships. JJVG thanks HG-recruitment, HG-Innovation "ECRAPS", HG-Innovation DSF, DASHH and CMWS for the financial support. We are grateful to Prof. Friščić for providing access to X-ray diffraction instrumentation. Portions of this research were carried out at the light source PETRA-III at DESY, a member of the Helmholtz Association (HGF). We would like to thank P11 staff for assistance in using beamline P11. We acknowledge the support of the Natural Sciences and Engineering Research Council of Canada (NSERC), [funding reference number: DGECR-2018-00344]. All MOF figures were made using VESTA 3.

Conflicts of interest

There are no conflicts to declare

Notes and references

1. O. M. Yaghi, M. O'Keeffe, N. W. Ockwig, H. K. Chae, M. Eddaoudi and J. Kim, *Nature*, 2003, **423**, 705-714.
2. A. K. Cheetham, G. Férey and T. Loiseau, *Angew. Chem. Int. Ed.*, 1999, **38**, 3268-3292.
3. J. Lee, O. K. Farha, J. Roberts, K. A. Scheidt, S. T. Nguyen and J. T. Hupp, *Chem. Soc. Rev.*, 2009, **38**, 1450-1459.
4. D.-X. Xue, Y. Belmabkhout, O. Shekhah, H. Jiang, K. Adil, A. J. Cairns and M. Eddaoudi, *J. Am. Chem. Soc.*, 2015, **137**, 5034-5040.
5. L. E. Kreno, K. Leong, O. K. Farha, M. Allendorf, R. P. Van Duyne and J. T. Hupp, *Chem. Rev.*, 2012, **112**, 1105-1125.
6. X. Zhang, M. A. Ballem, Z.-J. Hu, P. Bergman and K. Uvdal, *Angew. Chem. Int. Ed.*, 2011, **50**, 5729-5733.
7. N. W. Ockwig, O. Delgado-Friedrichs, M. O'Keeffe and O. M. Yaghi, *Acc. Chem. Res.*, 2005, **38**, 176-182.
8. M. A. Alnaqbi, A. Alzamly, S. H. Ahmed, M. Bakiro, J. Kegere and H. L. Nguyen, *J. Mater. Chem. A*, 2021, **9**, 3828-3854.
9. L.-L. Kang, M. Xue, Y.-Y. Liu, Y.-H. Yu, Y.-R. Liu and G. Li, *Coord. Chem. Rev.*, 2022, **452**, 214301.
10. D. J. Tranchemontagne, J. L. Mendoza-Cortés, M. O'Keeffe and O. M. Yaghi, *Chem. Soc. Rev.*, 2009, **38**, 1257-1283.
11. F. Saraci, V. Quezada-Novoa, P. R. Donnarumma and A. J. Howarth, *Chem. Soc. Rev.*, 2020, **49**, 7949-7977.
12. V. Guillerm, Ł. J. Weseliński, Y. Belmabkhout, A. J. Cairns, V. D'Elia, Ł. Wojtas, K. Adil and M. Eddaoudi, *Nat. Chem.*, 2014, **6**, 673-680.
13. L. Zhang, S. Yuan, L. Feng, B. Guo, J.-S. Qin, B. Xu, C. Lollar, D. Sun and H.-C. Zhou, *Angew. Chem. Int. Ed.*, 2018, **57**, 5095-5099.
14. Z. Chen, S. L. Hanna, L. R. Redfern, D. Alezi, T. Islamoglu and O. K. Farha, *Coord. Chem. Rev.*, 2019, **386**, 32-49.
15. H. Furukawa, F. Gándara, Y.-B. Zhang, J. Jiang, W. L. Queen, M. R. Hudson and O. M. Yaghi, *J. Am. Chem. Soc.*, 2014, **136**, 4369-4381.
16. R. C. Klet, Y. Liu, T. C. Wang, J. T. Hupp and O. K. Farha, *J. Mater. Chem. A*, 2016, **4**, 1479-1485.
17. A. H. Valekar, K.-H. Cho, S. K. Chitale, D.-Y. Hong, G.-Y. Cha, U. H. Lee, D. W. Hwang, C. Serre, J.-S. Chang and Y. K. Hwang, *Green Chem.*, 2016, **18**, 4542-4552.
18. R. J. Drout, A. J. Howarth, K.-i. Otake, T. Islamoglu and O. K. Farha, *CrystEngComm*, 2018, **20**, 6140-6145.
19. Y. Wang, L. Feng, W. Fan, K.-Y. Wang, X. Wang, X. Wang, K. Zhang, X. Zhang, F. Dai, D. Sun and H.-C. Zhou, *J. Am. Chem. Soc.*, 2019, **141**, 6967-6975.
20. P. R. Donnarumma, S. Frojmovic, P. Marino, H. A. Bicalho, H. M. Titi and A. J. Howarth, *Chem. Commun.*, 2021, **57**, 6121-6124.
21. R. Luebke, Y. Belmabkhout, Ł. J. Weseliński, A. J. Cairns, M. Alkordi, G. Norton, Ł. Wojtas, K. Adil and M. Eddaoudi, *Chem. Sci.*, 2015, **6**, 4095-4102.
22. J. P. Vizuet, M. L. Mortensen, A. L. Lewis, M. A. Wunch, H. R. Firouzi, G. T. McCandless and K. J. Balkus, *J. Am. Chem. Soc.*, 2021, **143**, 17995-18000.
23. J. Luo, H. Xu, Y. Liu, Y. Zhao, L. L. Daemen, C. Brown, T. V. Timofeeva, S. Ma and H.-C. Zhou, *J. Am. Chem. Soc.*, 2008, **130**, 9626-9627.
24. B.-X. Dong, X.-J. Gu and Q. Xu, *Dalton Trans.*, 2010, **39**, 5683-5687.
25. X. Liu, K. O. Kirlikovali, Z. Chen, K. Ma, K. B. Idrees, R. Cao, X. Zhang, T. Islamoglu, Y. Liu and O. K. Farha, *Chem. Mater.*, 2021, **33**, 1444-1454.
26. E. Aunan, C. W. Affolter, U. Olsbye and K. P. Lillerud, *Chem. Mater.*, 2021, **33**, 1471-1476.
27. B. Garai, V. Bon, F. Walenszus, A. Khadiev, D. V. Novikov and S. Kaskel, *Cryst. Growth Des.*, 2021, **21**, 270-276.
28. D. Feng, Z.-Y. Gu, J.-R. Li, H.-L. Jiang, Z. Wei and H.-C. Zhou, *Angew. Chem. Int. Ed.*, 2012, **51**, 10307-10310.
29. J. E. Mondloch, W. Bury, D. Fairen-Jimenez, S. Kwon, E. J. DeMarco, M. H. Weston, A. A. Sarjeant, S. T. Nguyen, P. C. Stair, R. Q. Snurr, O. K. Farha and J. T. Hupp, *J. Am. Chem. Soc.*, 2013, **135**, 10294-10297.